Characterization of the SARS-CoV-2 Spike in an Early Prefusion Conformation

Tingting Li[1,2,#], Qingbing Zheng[1,2,#], Hai Yu[1,2,#], Dinghui Wu[3,#], Wenhui Xue[1,2,#], Yuyun Zhang[1,2], Xiaofen Huang[1,2], Lizhi Zhou[1,2], Zhigang Zhang[1,2], Zhenghui Zha[1,2], Tingting Chen[1,2], Zhiping Wang[1,2], Jie Chen[1,2], Hui Sun[1,2], Tingting Deng[1,2], Yingbin Wang[1,2], Yixin Chen[1,2], Qingjian Zhao[1,2], Jun Zhang[1,2], Ying Gu[1,2,*], Shaowei Li[1,2,*], Ningshao Xia[1,2,*]

[1] State Key Laboratory of Molecular Vaccinology and Molecular Diagnostics, School of Life Sciences, School of Public Health, Xiamen University, Xiamen, China 361102

[2] National Institute of Diagnostics and Vaccine Development in Infectious Disease, Xiamen University, Xiamen, China 361102

[3] Department of Pulmonary Medicine, The First Affiliated Hospital of Xiamen University, Xiamen, China 361003

[#] T.L., Q.Z., D.W., H.Y. and W.X. contributed equally to this work.

[*] To whom correspondence may be addressed. E-mail: (Y.G.) guying@xmu.edu.cn or (S.L.) shaowei@xmu.edu.cn or (N.X.) nsxia@xmu.edu.cn

Running title: SARS-CoV-2 spike in an early prefusion conformation

Abstract

Pandemic coronavirus disease 2019 (COVID-19) is caused by the emerging severe acute respiratory syndrome coronavirus 2 (SARS-CoV-2), for which there are no efficacious vaccines or therapeutics that are urgently needed. We expressed three versions of spike (S) proteins—receptor binding domain (RBD), S1 subunit and S ectodomain—in insect cells. RBD appears monomer in solutions, whereas S1 and S associate into homotrimer with substantial glycosylation. The three proteins confer excellent antigenicity with six convalescent COVID-19 patient sera. Cryo-electron microscopy (cryo-EM) analyses indicate that the SARS-CoV-2 S trimer dominate in a unique conformation distinguished from the classic prefusion conformation of coronaviruses by the upper S1 region at lower position ~15 Å proximal to viral membrane. Such conformation is proposed as an early prefusion state for the SARS-CoV-2 spike that may broaden the knowledge of coronavirus and facilitate vaccine development.

Key words: COVID-19, SARS-CoV-2, spike, cryo-electron microscopy, antigenicity, early prefusion conformation

Introduction

The novel coronavirus grouped in betacoronavirus genus has become the third serious virus intruder to human in the coronaviridae, after sever acute respiratory syndrome coronaviruses (SARS-CoV) and middle east respiratory syndrome coronavirus (MERS-CoV), recently named SARS-CoV-2. In the phylogenic tree of the coronaviruses, SARS-CoV-2 is genetically close to some bat coronavirus and SARS-CoV, however, with its origin undefined[1]. SARS-CoV-2 causative disease "Coronavirus disease 2019" (abbreviated "COVID-19") is characterized by high fever, dry cough, difficulty breathing and sever atypical pneumonia, which usually be confirmed by virus RNA positive or pulmonary computed tomography (CT) in clinical practice[2, 3]. In terms of higher human-to-human transmissibility, SARS-CoV-2 has spread over 118 countries and areas, and led to over 125,288 confirmed cases worldwide and at least 4,614 deaths, as of March 12th 2020. The World Health Organization (WHO) has declared the SARS-CoV-2 epidemic as a pandemic of international concern and updates the COVID-19 situation every day.

SARS-CoV-2 is an enveloped, single and positive-stranded RNA virus encapsulated with a genome of ~30 kb. At least three membrane proteins including the surface spike protein (S), an integral membrane protein (M), a membrane protein (E). Like other coronaviruses, S is responsible for initiating the engagement to a specific cellular receptor angiotensin-converting enzyme 2 (ACE2) and mediating the cell-virus membrane fusion by the class I fusion mechanism[4, 5]. Thus, S is the main target for neutralizing antibodies against viral infection and the core immunogen constituent of

62 vaccine design. S is consisted of S1 and S2 subunits and the cleavage on S1/S2
63 boundary by protease during biosynthesis is prerequisite for coronaviruses cellular
64 membrane fusion and subsequent infection[6]. SARS-CoV-2 evolves a 4-residue
65 insertion (RRAR) as potential furin cleavage site rather than SARS-CoV and other bat
66 coronaviruses, which may contribute to the higher transmissibility of this novel
67 coronavirus[6, 7]. Previous studies suggested the infection process of MERS-CoV[8] and
68 SARS[9] viruses, where S trimer undergoes conformational transition from a prefusion
69 conformation ready for ACE2 binding to a postfusion conformation for eventual virus-
70 cell membrane fusion. Structure determination of SARS-CoV and MERS-CoV spike
71 trimers captured a variety of scenarios in the prefusion conformation showing partial
72 (one or two) receptor-binding domain (RBD) in the "up" conformation and the rest in
73 the "down", and all in either "up" or "down". The conformation transition from "down"
74 to "up" could expose the receptor binding site, and the subsequent receptor engagement
75 would lead to a substantial conformation rearrangement of S trimer from prefusion
76 conformation to postfusion. Two recent studies[7, 10] reported cryo-electron microscope
77 (cryo-EM) structures of SARS-CoV-2 spike trimers in the prefusion conformation with
78 2 RBDs down and 1 RBD up. In the case of SARS-CoV, this conformational change
79 during RBDs "down" to "up" was associated with the binding of receptor ACE2 as well
80 as the recognition of neutralizing monoclonal antibodies [11].

81 A safe and efficacious vaccine is urgently needed to control and eliminate the
82 SARS-CoV-2 infection. Various forms of vaccine candidates, mostly aiming to elicit
83 neutralizing antibodies against S proteins, are under preclinical research or even

84 subjected to clinical trials[12]. Here, we cloned S ectodomain and its fragments RBD and
85 S1 into recombinant baculovirus and expressed the proteins in insect cells. We found
86 that S and S1 formed homotrimer in solutions and the three proteins reacted well with
87 COVID-19 convalescent human sera. Cryo-EM analysis demonstrated the S trimer
88 unexpectedly retains a unique conformation distinguished from the classic prefusion
89 conformation of coronavirus spikes, that may represent an early state rather than the
90 known prefusion conformation of S spike. These results might broaden the knowledge
91 on coronavirus virology and provide another protective conformation of S trimer for
92 structure-based vaccine design against SARS-CoV-2 infection and its causative
93 COVID-19.
94
95 **Results**
96 **Construct design, expression and purification of SARS-CoV-2 S proteins**
97 To screen a potent immunogen for COVID-19 vaccine development, we designed three
98 constructs—S ectodomain, S1 and RBD—for the SARS-CoV-2 Spike (S) protein
99 expression by aligning the SARS-CoV-2 S gene (Genbank accession no. NC_045512.2)
100 to a SARS-CoV strain (Genbank accession no. NC_004718) S gene sequence in terms
101 of structure-defined domain profile of the SARS-CoV S protein (Fig. 1A). The gene of
102 SARS-CoV-2 S ectodomain encoding amino acids (aa) 15-1,213 with removal of its
103 original signal sequence was cloned to the downstream of the gp67 signal sequence in
104 pAcgp67B plasmid vector (Fig.1B). and with its C-terminal addition of a thrombin
105 cleavage site, a T4 trimerization foldon motif and his tag. The segments S1 (aa 15-

106 680) and RBD (aa 319-541) were cloned similar to S ectodomain, keeping gp67 signal
107 peptide and his tag to facilitate secretory outside cell and affinity purification,
108 respectively, but without the thrombin site and T4 foldon (Fig. 1A). The three
109 constructed plasmids were respectively co-transfected into Sf9 insect cells with v-
110 cath/chiA gene deficient baculovirus DNA for the generation and amplification of
111 recombinant baculovirus, which were then harnessed to infect Hive Five insect cells to
112 eventually produce recombinant proteins, named S, S1 and RBD respectively.

113 The recombinant proteins were mostly soluble expressed and secreted into the
114 culture medium. The centrifugation supernatants of cell culture went through metal
115 affinity chromatography using Ni-NTA resin. S, S1 and RBD proteins were mainly
116 eluted in a separation fractions under 250 mM imidazole elution, and resolved as
117 molecular weight (m.w.) of ~180 kDa, 110 kDa and 35 kDa, respectively, in SDS-
118 PAGE as indicated by a corresponding western blotting (WB) using anti-His antibody
119 as detection antibody (Fig. 1C). Interestingly, about one half S proteins were cleaved
120 into S1 (identical migration site to S1 lane in Fig. 1C) and S2 (about 80kDa developed
121 in anti-His WB) possibly by innate furin of insect cell that was also found in other cases
122 of enzymatic cleave while protein expression in insect cell, such as Flu HA [13]. The
123 eluted S fraction was further polished by Superdex 200 to remove contaminative
124 proteins (Fig. 1D). These peaks fractionated at retention volume 28mL, 36mL, 48mL,
125 and 65mL, were further harvested and subjected to SDS-PAGE analysis. The results
126 indicated that S proteins together with cleaved S1/S2 were resolved at peak 1 in size-
127 exclusion chromatography (Fig. 1D) and showed a high purity of over 95% total

128 S/S1/S2 in gel (Fig. 1E). Overall, one-step Ni-NTA affinity chromatography produced
129 RBD with 95% purity and a yield of 30 mg per L cell culture, S1 with about 90% purity
130 and 10 mg per L yield, while further purification through a size-exclusion
131 chromatography (SEC), the resultant S sample had over 95% purity regarding intact S
132 and cleaved S1/S2, and was harvested in a yield of 1 mg per L cell culture. These data
133 set up a start point for further optimization on expression and purification process of
134 SARS-CoV-2 S immunogen candidates through insect baculovirus expression vector
135 system (BEVS).
136
137 **Physiochemical properties of SARS-CoV-2 S-RBD, S1 and S proteins**
138 We next investigated the physiochemical properties of the recombinant S protein and
139 its fragments purified from insect cells, including association potential, thermal
140 stability and glycosylation situation. Firstly, high pressure size-exclusion
141 chromatography (HPSEC) and sedimentation velocity analytical ultracentrifugation
142 (SV-AUC) analyses were carried out to measure the oligomerization potential of the
143 three proteins in solution. RBD, S1 and S all showed single major peak in HPSEC
144 profiles at elution volume of 9.0 mL, 5.5 and 5.3 mL, respectively (Fig. 2A and Fig.
145 2B). RBD, S1 and S were further verified by SV-AUC, where RBD sedimented as
146 single species of 3.1S in c(s) profile, corresponding to apparent molecular weight 22
147 kDa (Fig. 2D); S1 existed as a dominant species of 11.3 S (estimated as 277 kDa
148 corresponding to S1 trimer) and a minor aggregate form of 20 S (Fig. 2E); S and cleaved
149 S1/S2 resolved as 15.2 S, equivalent to 577 kDa, approximately as the theoretical

150 molecular weight of intact S trimer. The three proteins were further analyzed by
151 differential scanning calorimetry (DSC) that was usually used to investigate the inner
152 thermostability of macromolecules or their complexes[14]. RBD and S1 showed one
153 major peak at comparable thermal denaturation midpoints (Tm) of 46.0 °C and 45.5 °C,
154 respectively (Fig. 3G and 3H), whereas S sample showed two major peaks at Tm of
155 45.5°C (identical to Tm of S1) and 64.5°C (Fig. 3I), which might reflect the coexistence
156 of intact S and cleaved S1/S2.

157 On the other hand, we investigated the glycosylation extent of the three protein by
158 enzymatic deglycosylation analysis. Endo H could unleash the chithobiose core of high
159 mannose and some hybrid oligosaccharides from N-liked glycoproteins, therefore
160 remove the extended branches of glycans and leave the one N acetylglucosamine
161 (GlcNAc) on N-linked glycoproteins. While PNGase F would release N-linked glycan
162 moieties between GlcNAc and ASN residues within a glycoprotein. It should be noted
163 that glycosylation in insect cells is featured as terminal mannose glycans, unlike
164 complex sialylated glycans in mammalian cells, and glycosylation is known to correlate
165 the immunogenicity and broad-coverage protection of a glycoprotein immunogen[15, 16].
166 After the treatment of either Endo H or PNGase F, RBD showed no discernible decrease
167 of molecular weight in SDS-PAGE/anti-His WB, S1 and S2 both demonstrated nearly
168 ~10 kDa decrease, and the intact S exhibited substantial shrinkage in molecular weight
169 of about ~20 kDa decrease (Fig. 2J). The analyses conclude that the glycosylation
170 extent within S glycoprotein is RBD < S1 ~ S2, consistent to the predicted glycosylation
171 profile of S polypeptide (Fig. 1A).

172

173 **Reactivity of SARS-CoV-2 RBD, S1 and S proteins against convalescent COVID-**

174 **19 human sera**

175 We next evaluated the antigenicity of the three versions of S proteins by WB and ELISA

176 using a panel of six COVID-19 convalescent human sera, which was collected from

177 COVID-19 patients after they recovered from the disease in the First Affiliated Hospital

178 of Xiamen University. Eight reducing SDS gel duplicates of the one depicted in Fig.

179 1C were prepared for WB analysis using these six convalescent sera and two control

180 sera from health human (Fig. 3A-3H, left panel). As expected, intact S protein bands

181 reacted well with all the six convalescent sera (Fig. 3A-3H, left panel). Unexpectedly,

182 five of six sera showed no or very weak reactivities against RBD, only Serum #6

183 possessed RBD's activity. Among the five sera with lower RBD-reactivity, Serum #2,

184 #3 and #5 well recognized S1 and the cleaved S1 in lane S, suggesting these sera may

185 specifically react with NTD of S1. S2 demonstrated reaction activity against all the six

186 sera, like the intact S. No detectable reaction was observed in the control sera (Fig. 3G

187 and 3H). Inconsistent to the WB results, RBD, S1 and S shared comparable reactivities

188 against the convalescent sera in ELISA, although the sera per se presented varied

189 reaction titers (represented as ET50) following the reaction sequence: Serum #5 > #2 >

190 #3> #1 > # 6 > #4 (Fig. 3A-3H, right panel).

191 Taken together, RBD, S1 and S proteins from insect cells maintain the native-like

192 SARS-CoV-2 epitopes. These epitopes in native virion should be immunogenic in

193 COVID-19 patients and capable of eliciting high antibody titer in the convalescent

194 phase of SARS-CoV-2 infection. Among these epitopes, most RBD epitopes are strictly
195 tertiary conformation-dependent sites that are damaged upon the mild denatured
196 condition of reductant and SDS treatment, NTD within S1 bears some linear epitopes,
197 whereas S2 part essentially has linear epitopes that are immunogenic in all COVID-19
198 patients (n=6).
199

200 **Cryo-EM structures of SARS-CoV-2 S proteins**

201 To examine the structure of the trimeric S ectodomain with native sequence, we
202 prepared cryo-EM grids using the Ni-NTA purified S proteins and collected 1,513
203 electron micrograph movies. Most of motion-corrected micrographs demonstrated
204 plenty of well-dispersed particles with an approximate size as the canonical coronavirus
205 S trimer (Fig. 4A). A total of 162,645 particles were picked out for multiple rounds of
206 2D classification, consequently, 37,147 particles grouped into top 10 classes, rendering
207 typical feature of S trimer in prefusion conformation as recently reported[7, 10], were
208 selected for further analysis (Fig. 4B). 3D reconstruction (applying 3-fold symmetry)
209 yielded the density map of prefusion spike (S-pre) at resolution of 5.43 Å (Fig. 3D and
210 Supplementary Fig. 1A).

211 Structurally, three S monomers intertwine around each other and associate to
212 homotrimers with 145 Å height seen from side-view and 160 Å diameter in top-view
213 (Fig. 4C and 4D). We then recruited the recently reported cryo-EM map of S prefusion
214 trimer (EMD-21374, at resolution of 3.17 Å, low pass to 5.43 Å prior to structural
215 comparison) and compared our cryo-EM map at same resolution (Fig. 4D). It was

worthy noted that the compared prefusion SARS-CoV-2 S trimer was engineered with site-directed mutations to stabilize prefusion conformation and expressed in 239F cells. The mutant included two stabilizing proline mutations at residues 986, 987 and a "GSAS" substitution at the furin cleavage site[7]. Surprisingly, the alignment demonstrated that the two cryo-EM structures share similar mushroom-shaped architecture in particular nearly identical at stalk moiety (S2 region), but our S-pre shows the cap part (S1 region) at ~15Å lower position than the reported S trimer in RBD-down prefusion conformation (Fig. 4D). Regarding to substantial mismatch at the density of 3 S1 subunits, we respectively fitted 5 individual domains (NTD, RBD, SD1, SD2 and S2) of the SARS-CoV-2 S structure (PDB code 6VSB) to our S-pre map. In the fitting map, NTD, RBD, SD2 and S2 could be well placed in the S-pre map, especially for the latter two, which reflects the aforementioned good match at the stalk of the mushroom-shape (Supplementary Fig. 2). However, there is no observable density between RBD and SD2 to accommodate an SD1 model (Supplementary Fig. 2), which suggests SD1 region is dramatically flexible in our S-pre structure (Fig. 4E and 4F). When the combined model of fitted NTD-RBD-SD2-S2 was superimposed to the original S protomer structure (PDB code 6VSB, Chain A, RBD in down conformation), both NTD and RBD in the original S obviously move and rotate up against our combined model (Fig. 4G). The structural comparison demonstrated that the S-pre trimer retains a unique conformation different from the prefusion conformation of the two reported SARS-CoV-2 spike structures (PDB codes 6VSB and 6VXX).

237 We then compared the conformation of our S-pre structure with that of 21
238 deposited coronavirus S models. Six representative S structures[7, 17-20] from four known
239 genus (α-, β-, γ- and δ-genus) in coronaviridae are respectively fitted to the S-pre map
240 (Supplementary Fig. 3). Five S trimer structures of other coronaviruses share similar
241 prefusion conformation with the reported SARS-CoV-2 S structure but substantially
242 distinct with the unique conformation of our S-pre.

243 Apart from most particles classified as S-pre in our sample, 2D classifications also
244 showed five classes of few particles (2,951) assuming an elongated rosette-shape
245 assembly. These particles were further reconstructed and yielded a structure at lower
246 resolution of 8.40 Å (Supplementary Fig. 1B) that could be considered as post-fusion
247 spike (S-post), as the structure has similar shape but shorter length (~170 Å) as
248 compared to the postfusion spike of SARS-CoV[21] and the presumed one observed in
249 native SARS-CoV-2 virion (BioRxiv, https://doi.org/10.1101/2020.03.02.972927)
250 (Supplementary Fig. 4) . Fitting the S-post map with the core region structure of SAR-
251 CoV-2 S2 subunit in post-fusion conformation (PDB code 6LXT) indicated that our S-
252 post exhibits roughly rod shape similar with the post-fusion structure (Supplementary
253 Fig. 4).

254

255 **Conformational transition of SARS-CoV-2 spike from early prefusion to**
256 **postfusion**

257 Briefly, we've obtained two conformations of SARS-CoV-2 spike from insect cells.
258 The dominant one maintains the similar mushroom-shaped trimer as the previous

models, while the S1 region substantially diverges. The other conformation essentially resembles the postfusion state. However, we could not find the classic prefusion conformation in our sample. We next tried to figure out at which stage the unique conformation occurs during the spike conformation change. The space relationship of NTD or RBD to S2 domain in the unique, RBD-down and RBD-up prefusion conformations (Fig. 5A) was measured by a reference plant approximately parallel to the viral membrane. The plane is defined by the positions of three equivalent Cα atoms (residue 694 be used) from three S2 subunits of the trimer structures. Numerical data shows that (1) the NTD and RBD in the unique conformation retain the lowest position in the three prefusion conformations; (2) the NTD and RBD of RBD-down prefusion stretch upward 16.6° rotation/16 Å elevation, and 13.1°/18 Å, respectively, with respect to the unique conformation; (3) from RBD-down to RBD-up prefusion state, the RBD elevates 9 Å with an additional rotation whereas the NTD remaining nearly stationary (Supplementary Movie S1). The resultant "up" RBD is ready for ACE2 binding and the spike eventually is rearranged to postfusion state upon RBD-ACE2 interaction[11, 22] (Fig. 5B). The motion trend of NTD and RBD from prefusion to postfusion state in conformational transition is away from the viral membrane, suggesting the unique conformation may occur earlier than RBD-down prefusion conformation, named as "early prefusion conformation" (Fig. 5). This early prefusion conformation might exist in other coronaviruses as well.

281 **Discussion**

282 SARS-CoV-2 has crossed the species barrier and sweep over the planet by person-to-
283 person transmission in an R0 ~2.56 rate[23], first wave in China and the second wave
284 booming outside China. WHO has declared the event as another pandemic infectious
285 disease in human history, and the epidemiology of SARS-CoV-2 infection is still in
286 data accumulation. Although the biology and virology of SARS-CoV-2 remain elusive,
287 in terms of knowledge on other coronaviruses, the spikes decorating the SARS-CoV-2
288 virion play a critical role in viral attachment and entry to host cells. Cryo-EM structures
289 of spikes in the prefusion conformation, and RBD-bound receptor ACE2 have indicated
290 the engagement of SARS-CoV-2 to cellular membrane requires a serial of
291 conformational change of RBDs. The change is presumed from the start point of 3
292 RBDs down in the prefusion conformation, then RBD(s) up for ACE2 binding, and
293 eventually spike is rearranged to postfusion. In this study, we suggest that the SARS-
294 CoV-2 spike may retain at more precedent state than the classic prefusion conformation
295 that has been determined for other coronaviruses. This early prefusion conformation
296 features that the cap of the mushroom-shaped spike constituted by three S1 subunits is
297 more proximal to viral membrane by 15 Å than in the classic prefusion conformation.

298 The SARS-CoV-2 spike expressed in insect cells predominantly retains a unique
299 early prefusion conformation, which was repeatable in at least three batches of samples
300 and is ascribed to two possible reasons – native aa sequence used in the S ectodomain
301 construct and over-expression in insect cells. There is about a half of S proteins
302 undergoing cleavage on the S1/S2 boundary site in the purified samples both after the

303 first Ni-NAT and the second SEC purification (Fig. 1C and 1E). Further analyses
304 suggest the split between S1 and S2 likely takes no effect on the trimerization of S
305 trimer. It is known that the insect cells can confer post-translation glycosylation for
306 protein over-expression as mammalian cells despite the latter can produce more
307 complex sialyation[24], and thus provide an alternative way to generate glycoprotein in
308 native conformation. Our results indicate that RBD, NTD and S2 domains of SARS-
309 CoV-2 demonstrated different glycosylation extent in insect cells, however, RBD, S1
310 and S proteins comparably react well with six convalescent COVID-19 human sera
311 albeit they differ in domain composition, polypeptide length and oligomerization.

312 There are numbers of SARS-CoV-2 vaccine candidates, including inactivated,
313 vectored, recombinant and nucleotide vaccine forms, under preclinical research.
314 Various versions of S proteins are the major targets for vaccine immunogen candidate.
315 In addition to potent neutralizing antibody elicitation upon immunization, potential
316 antibody-dependent disease enhancement (ADE) is the major concern for an efficacious
317 SARS-CoV-2 vaccine. ADE has been found in the development of numbers of virus
318 vaccine candidates, including respiratory syndrome virus (RSV), dengue fever [25, 26],
319 human immunodeficient virus (HIV), SARS-CoV, MERS-CoV [25-27] and so on. It is
320 believed that ADE is associated with non-neutralization epitope attribute and / or
321 specific antibody isotype[28, 29], in which virus-bound antibody would promote the viral
322 infection to immune cells through Fc fragment targeting γFc receptors on the cellular
323 surface and enhance the disease severity. Therefore, the strategy of vaccine design
324 against SARS-CoV-2 should include the consideration of antigen region selection,

325 glycosylation number/extent and exactly presented prefusion conformation. The
326 prefusion conformation needed to be maintained is exemplified by the case of RSV
327 vaccine candidate in which F trimer in prefusion is much potent than postfusion. Hence
328 the early prefusion conformation proposed for SARS-CoV-2 spike should be drawn an
329 attention for immunogen design as well as the prefusion one.

330 In conclusion, we obtain three kinds of S proteins showing excellent antigenicity
331 and find an early prefusion conformation for SARS-CoV-2 spike. Nevertheless, the
332 molecular level detail for such conformation and the underlying immunogenicity
333 should be further investigated, and whether this conformation recapitulates the exact
334 state of spike in native SARS-CoV-2 virion remains to be determined.

335

336 **Materials and Methods**

337 **Cloning, protein expression and purification**

338 The SARS-CoV-2 S gene (Genbank accession no. NC_045512.2) was synthesized and
339 cloned into a baculovirus shuttle vector pAcgp67B (BD Biosciences, CA, USA) using
340 Gibson assembly. The S construct encoding aa 15-1,213 (numbered as original
341 sequence), contains a thrombin site, a T4 foldon domain to assist in trimerization and a
342 C-terminal 10-His tag for purification. For S1 construct contains gene encoding aa 15-
343 680 followed by a 10-His tag. The RBD construct (aa 319-541) also contains 10-his tag
344 to facilitate purification. In all three constructs, the natural signal peptide (aa 1-14
345 analyzed by SignalP tool) was replaced with a gp67 secretion signal peptide at N-
346 terminus.

347 The expression and purification of proteins were performed as described
348 previously[30]. All plasmids were co-transfected with linearized 2.0 DNA (deficient in *v-*
349 *cath/chiA*genes) (Expression Systems, CA, USA) into *Sf9* insect cells (Thermo Fisher
350 Scientific, MA, USA), according to the protocol provided by the manufacturer
351 (Expression Systems). The transfection supernatant was harvested and amplified 2
352 times to obtain a high titer of the recombinant viruses. Hive Five cells (BTI-TN-5B1-
353 4) (Thermo Fisher Scientific) were cultured in ESF921 medium (Expression Systems)
354 and infected with recombinant virus at an multiplicity of infection (MOI) of 5 in the
355 exponential growth phase (2× 106 cells/ml, 95% viability) at 28°C for 72 h. The culture
356 media was centrifugated at 8,000 rpm for 20 min. Then the supernatant was dialyzed
357 against phosphate-buffered saline (PBS), pH 7.4, and purified with Ni-sepharose fast
358 flow 6 resin (GE Healthcare, Boston, USA) by the elution with 250 mM imidazole. The
359 protein concentrations of the final purified samples were measured with Pierce™BCA
360 Protein Assay Kit (Thermo Fisher Scientific).
361
362 **SDS-PAGE and western blot**
363 Protein samples were mixed with loading buffer and boiled for 10 min, and subjected
364 to sodium dodecyl sulfate-polyacrylamide gel electrophoresis (SDS-PAGE). Equal
365 amounts of proteins for each sample were loaded onto two SDS-PAGE gels, one for
366 western blotting and one for Coomassie staining. The proteins were electrophoresed for
367 70 min at 80 V in a BioRad MINI-PROTEAN Tetra system (BioRad Laboratories, CA,
368 USA), and the gel was stained with Coomassie Brilliant Blue R-250 (Bio-Rad) for 30

369 min at room temperature. For western blotting, separated proteins were transferred onto
370 a nitrocellulose membrane (Whatman, Dassel, Germany) using a Trans-Blot Turbo
371 transfer system (Bio-Rad). The membrane was blocked and then incubated for 1 h with
372 an His-tag-specific mouse mAb antibody (Proteintech, Rosemont, USA) or human sera
373 (1:500 dilution). Unbound antibody was removed by five 5-min washes and the
374 membrane was incubated with alkaline phosphatase-conjugated goat anti-mouse
375 secondary antibody or goat anti-human IgG secondary antibody (Abcam, Cambridge,
376 UK). Membranes were washed again and then developed using SuperSignal ELISA
377 Pico Chemiluminescent Substrate Kit (Thermo Fisher Scientific).
378
379 **Enzyme-Linked Immunosorbent Assay (ELISA)**
380 Purified proteins were coated onto 96-well microtiter plates at 100 ng/well in PBS at
381 37°C for 4 h. The background was blocked with 1 × Enzyme dilution buffer (PBS +
382 0.25% casein + 1% gelatin + 0.05% proclin-300) at 37°C for 2 h. Sera were diluted
383 started at 1:100 followed with three-fold serially dilution, and added to the wells (100 μl)
384 and incubated at 37°C for 1 h. Horseradish peroxidase (HRP)-labeled mouse anti-
385 human antibody (Abcam) was used as secondary antibody at 1:5,000 for 30 min. Wells
386 were washed again and the reaction catalyzed using o-phenylenediamine (OPD)
387 substrate at 37°C for 10 min. The OD450nm (reference, OD620nm) was measured on
388 a microplate reader (TECAN, Männedorf, Switzerland), with a cut-off value 0.1. The
389 Half effective titers (ET50) was calculated by sigmoid trend fitting using GraphPad
390 Prism software.

391 **Size-Exclusive Chromatography (SEC)**

392 Ni-NTA purified S proteins were further loaded into Superdex200 (GE Healthcare), the
393 fractions were harvested and analyzed by SDS-PAGE. All high-purity RBD, S1 and S
394 proteins were subjected to HPLC (Waters; Milford, MA) analysis using a TSK Gel
395 G5000PWXL7.8 × 300 mm column (TOSOH, Tokyo, Japan) equilibrated in PBS, pH
396 7.4. The system flow rate was maintained at 0.5 mL/min and eluted proteins were
397 detected at 280 nm.

398

399 **Analytical Ultracentrifuge (AUC)**

400 The AUC assay was performed using a Beckman XL-Analytical ultracentrifuge
401 (Beckman Coulter, Fullerton, CA), as described elsewhere[31]. The sedimentation
402 velocity (SV) was carried out at 20°C with diluted proteins in PBS. The AN-60 Ti rotor
403 speed was set to 20,000-30,000 rpm according to the molecular weight of the control
404 proteins. Data was collected using SEDFIT computer software, kindly provided by Dr.
405 P. C. Shuck (NIH, Bethesda, MA, USA). Multiple curves were fit to calculate the
406 sedimentation coefficient (S) using continuous sedimentation coefficient distribution
407 model [c(s)], and then the c(s) used to estimate protein molar mass.

408

409 **Differential scanning calorimetry (DSC)**

410 Differential scanning calorimetry (DSC) was carried out on the S proteins using a
411 MicroCal VP-DSC instrument (GE Healthcare, MicroCal Products Group,
412 Northampton, MA) as described previously[14]. In brief, all samples with a concentration

413 of 0.2 mg/mL were measured at a heating rate of 1.5°C /min with the scan temperature
414 ranging from 10°C to 90°C. The melting temperatures (Tm) were calculated using
415 MicroCal Origin 7.0 (Origin-Lab Corp., Northampton, MA) software assuming a non-
416 two-state unfolding model.
417
418 **Endo-H and PNGase-F digestion**
419 The Endo-H (NEB) and PNGase-F (NEB) digestions were performed according to the
420 protocol offered by instruction. In brief, the deglycosylation reactions were carried out
421 using 10ug S proteins with 5uL of Endo H or PNGase F and incubated at 37°C
422 overnights. The reactions were loaded in to SDS-PAGE and analyzed by Western
423 blotting using anti-His as detecting anybody.
424
425 **Cryo-EM sample preparation and data collection.**
426 Aliquots (3 μL) of 0.5 mg/mL purified SARS-CoV-2 S protein were loaded onto glow-
427 discharged (60 s at 20 mA) holey carbon Quantifoil grids (R1.2/1.3, 200 mesh,
428 Quantifoil Micro Tools) using a Vitrobot Mark IV (ThermoFisher Scientific) at 100%
429 humidity and 4°C. Data were acquired using the EPU software to control a FEI Tecnai
430 F30 transmission electron microscope (ThermoFisher Scientific) operated at 300 kV.
431 and equipped with a ThermoFisher Falcon-3 direct detector. Images were recorded in
432 the 58-frame movie mode at a nominal magnification of 93,000X with a pixel size of
433 1.12 Å. The total electron dose was set to 46 e^{-} $Å^{-2}$ and the exposure time was 1.5 s.

537 micrographs were collected with a defocus range comprised between 1.5 and 2.8 μm.

Cryo-EM data processing

Movie frame alignment and contrast transfer function estimation of each aligned micrograph were carried out with the programs Motioncor[32] and Gctf[33]. Particles were picked by the 'Templete picker' session of cryoSPARC v2[34]. Two rounds of reference-free 2D classification were performed and well-defined particle images were selected and non-uniform 3D refinement, 3D reconstruction with C3 symmetry were performed using cryoSPARC v2. The resolutions of the final maps were estimated on the basis of the gold-standard FSC curve with a cutoff at 0.143[35]. Density-map-based visualization and segmentation were performed with Chimera[36].

Acknowledgments

This work was supported by grants from the National Natural Science Foundation (grant no. U1705283, 31670935, 81971932, 81991491, 31730029), and the Major Project of Fujian Provincial Science Foundation for COVID-19 Research (Grants 2020YZ014001).

Financial Disclosure

The funders had no role in study design, data collection and analysis, decision to publish, or preparation of the manuscript.

Competing Interest

The authors have declared that no competing interests exist.

Author Contributions

Y.G, S.L. and N.X. designed the study. T.L., Q.Zheng., H.Y., D.W., W.X., Y.Z., X.H., L.Z., Z.Zhang., Z.Zhai., T.C., Z.W., J.C., H.S. and T.D. performed experiments. T.L., Q.Z., H.Y., Y.W., Y.C., Q.Zhao., J.Z., Y.G., S.L. and N.X. analyzed data. T.L., Q.Z., H.Y., Y.G., and S.L. wrote the manuscript. T.L., Q.Zheng., H.Y., D.W., W.X., Q.Zhao., J.Z. Y.G., S.L., and N.X. participated in discussion and interpretation of the results. All authors contributed to experimental design.

References

1 Chan JF, Kok KH, Zhu Z *et al.* Genomic characterization of the 2019 novel human-pathogenic coronavirus isolated from a patient with atypical pneumonia after visiting Wuhan. *Emerg Microbes Infect* 2020; **9**:221-236.

2 Zhu N, Zhang D, Wang W *et al.* A Novel Coronavirus from Patients with Pneumonia in China, 2019. *N Engl J Med* 2020; **382**:727-733.

3 Wang D, Hu B, Hu C *et al.* Clinical Characteristics of 138 Hospitalized Patients With 2019 Novel Coronavirus-Infected Pneumonia in Wuhan, China. *JAMA* 2020.

4 Zhou P, Yang XL, Wang XG *et al.* A pneumonia outbreak associated with a new coronavirus of probable bat origin. *Nature* 2020; **579**:270-273.

5 Wan Y, Shang J, Graham R, Baric RS, Li F. Receptor recognition by novel coronavirus from Wuhan: An analysis based on decade-long structural studies of SARS. *J Virol* 2020.

6 Millet JK, Whittaker GR. Host cell proteases: Critical determinants of coronavirus tropism and pathogenesis. *Virus Research*; **202**:120-134.

7 Wrapp D, Wang N, Corbett KS *et al.* Cryo-EM structure of the 2019-nCoV spike in the prefusion conformation. *Science (New York, NY)* 2020.

8 Walls AC, Xiong X, Park Y-JJ *et al.* Unexpected Receptor Functional Mimicry Elucidates Activation of Coronavirus Fusion. *Cell* 2019; **176**:1026.

9 Yuan Y, Cao D, Zhang Y *et al.* Cryo-EM structures of MERS-CoV and SARS-CoV spike

glycoproteins reveal the dynamic receptor binding domains. *Nature communications* 2017; **8**:15092.

10 Walls AC, Park Y-JJ, Tortorici MA, Wall A, McGuire AT, Veesler D. Structure, Function, and Antigenicity of the SARS-CoV-2 Spike Glycoprotein. *Cell* 2020.

11 Gui M, Song W, Zhou H *et al.* Cryo-electron microscopy structures of the SARS-CoV spike glycoprotein reveal a prerequisite conformational state for receptor binding. *Cell research* 2017; **27**:119-129.

12 Lu S. Timely development of vaccines against SARS-CoV-2. *Emerg Microbes Infect* 2020; **9**:542-544.

13 Sui J, Hwang WC, Perez S *et al.* Structural and functional bases for broad-spectrum neutralization of avian and human influenza A viruses. *Nature structural & molecular biology* 2009; **16**:265-273.

14 Zhang X, Wei M, Pan H *et al.* Robust manufacturing and comprehensive characterization of recombinant hepatitis E virus-like particles in Hecolin(®). *Vaccine* 2014; **32**:4039-4050.

15 Medina RA, Stertz S, Manicassamy B *et al.* Glycosylations in the globular head of the hemagglutinin protein modulate the virulence and antigenic properties of the H1N1 influenza viruses. *Science translational medicine* 2013; **5**.

16 Liu W-CC, Jan J-TT, Huang Y-JJ, Chen T-HH, Wu S-CC. Unmasking stem-specific neutralizing epitopes by abolishing N-linked glycosylation sites of influenza hemagglutinin proteins for vaccine design. *Journal of virology* 2016.

17 Walls AC, Tortorici MA, Frenz B *et al.* Glycan shield and epitope masking of a coronavirus spike protein observed by cryo-electron microscopy. *Nat Struct Mol Biol* 2016; **23**:899-905.

18 Yuan Y, Cao D, Zhang Y *et al.* Cryo-EM structures of MERS-CoV and SARS-CoV spike glycoproteins reveal the dynamic receptor binding domains. *Nature communications* 2017; **8**:15092.

19 Shang J, Zheng Y, Yang Y *et al.* Cryo-EM structure of infectious bronchitis coronavirus spike protein reveals structural and functional evolution of coronavirus spike proteins. *PLoS Pathog* 2018; **14**:e1007009.

20 Shang J, Zheng Y, Yang Y *et al.* Cryo-Electron Microscopy Structure of Porcine Deltacoronavirus Spike Protein in the Prefusion State. *J Virol* 2018; **92**.

21 Song W, Gui M, Wang X, Xiang Y. Cryo-EM structure of the SARS coronavirus spike glycoprotein in complex with its host cell receptor ACE2. *PLoS Pathog* 2018; **14**:e1007236.

22 Yan R, Zhang Y, Li Y, Xia L, Guo Y, Zhou Q. Structural basis for the recognition of the SARS-CoV-2 by full-length human ACE2. *Science (New York, NY)* 2020.

23 Zhao S, Musa SS, Lin Q *et al.* Estimating the Unreported Number of Novel Coronavirus (2019-nCoV) Cases in China in the First Half of January 2020: A Data-Driven Modelling Analysis of the Early Outbreak. *Journal of clinical medicine* 2020; **9**.

24 Palomares LA, Srivastava IK, Ramírez OT, Cox MMJMJ. Glycobiotechnology of the Insect Cell-Baculovirus Expression System Technology. *Advances in biochemical engineering/biotechnology* 2018.

25 Wang SF, Tseng SP, Yen CH *et al.* Antibody-dependent SARS coronavirus infection is mediated by antibodies against spike proteins. *Biochem Biophys Res Commun* 2014; **451**:208-214.

26 Wan Y, Shang J, Sun S *et al.* Molecular Mechanism for Antibody-Dependent Enhancement of Coronavirus Entry. *J Virol* 2020; **94**.

531 27 Kam YW, Kien F, Roberts A *et al.* Antibodies against trimeric S glycoprotein protect hamsters
532 against SARS-CoV challenge despite their capacity to mediate FcgammaRII-dependent entry into
533 B cells in vitro. *Vaccine* 2007; **25**:729-740.
534 28 Dejnirattisai W, Supasa P, Wongwiwat W *et al.* Dengue virus sero-cross-reactivity drives
535 antibody-dependent enhancement of infection with zika virus. *Nature immunology* 2016;
536 **17**:1102-1108.
537 29 Rey FAA, Stiasny K, Vaney M-CC, Dellarole M, Heinz FX. The bright and the dark side of human
538 antibody responses to flaviviruses: lessons for vaccine design. *EMBO reports* 2018; **19**:206-224.
539 30 Li T, Zhang Z, Zhang Z *et al.* Characterization of native-like HIV-1 gp140 glycoprotein
540 expressed in insect cells. *Vaccine* 2019; **37**:1418-1427.
541 31 Li Z, Wang D, Gu Y *et al.* Crystal Structures of Two Immune Complexes Identify Determinants
542 for Viral Infectivity and Type-Specific Neutralization of Human Papillomavirus. *mBio* 2017; **8**.
543 32 Zheng SQ, Palovcak E, Armache J-P, Verba KA, Cheng Y, Agard DA. MotionCor2: anisotropic
544 correction of beam-induced motion for improved cryo-electron microscopy. *Nature methods*
545 2017; **14**:331.
546 33 Zhang K. Gctf: Real-time CTF determination and correction. *Journal of structural biology* 2016;
547 **193**:1-12.
548 34 Punjani A, Rubinstein JL, Fleet DJ, Brubaker MA. cryoSPARC: algorithms for rapid unsupervised
549 cryo-EM structure determination. *Nat Methods* 2017; **14**:290-296.
550 35 Kucukelbir A, Sigworth FJ, Tagare HD. Quantifying the local resolution of cryo-EM density maps.
551 *Nature methods* 2014; **11**:63.
552 36 Pettersen EF, Goddard TD, Huang CC *et al.* UCSF Chimera—a visualization system for
553 exploratory research and analysis. *Journal of computational chemistry* 2004; **25**:1605-1612.

554

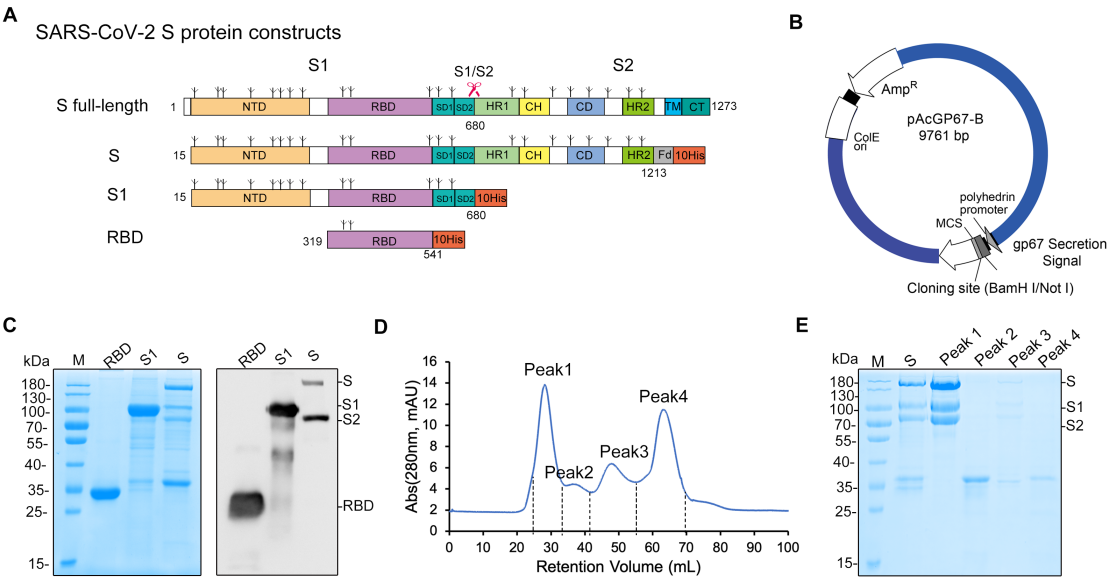

Figure 1. Schematic map of the SARS-CoV-2 S protein constructs. (A) Linear representations of the S protein primary structure and construct design. NTD, N-terminal domain; RBD, receptor binding domain; SD1, subdomain 1; SD2, subdomain 2; HR1, heptad repeat 1; CH, central helix; CD, connector domain; HR2, heptad repeat 2; TM, transmembrane domain; CT, cytoplasmic tail; FD, T4 foldon motif. The predicted glycosylation sites are indicated above the domain bars. (B) Map of the cloning vector pAcgp67B. The interest genes were cloned to plasmid pAcgp67B at BamH I/Not I site to generate transfer vectors. (C) SDS-PAGE and western blotting of the Ni-NTA purified proteins. RBS, S1 and S were eluted by 250 mM imidazole. Anti-His antibody was used as detection antibody in western blotting. (D) Size-exclusion chromatogram of the second-step purification of the S protein. (E) SDS-PAGE of the four fractions harvested from the chromatography purification as shown in (D).

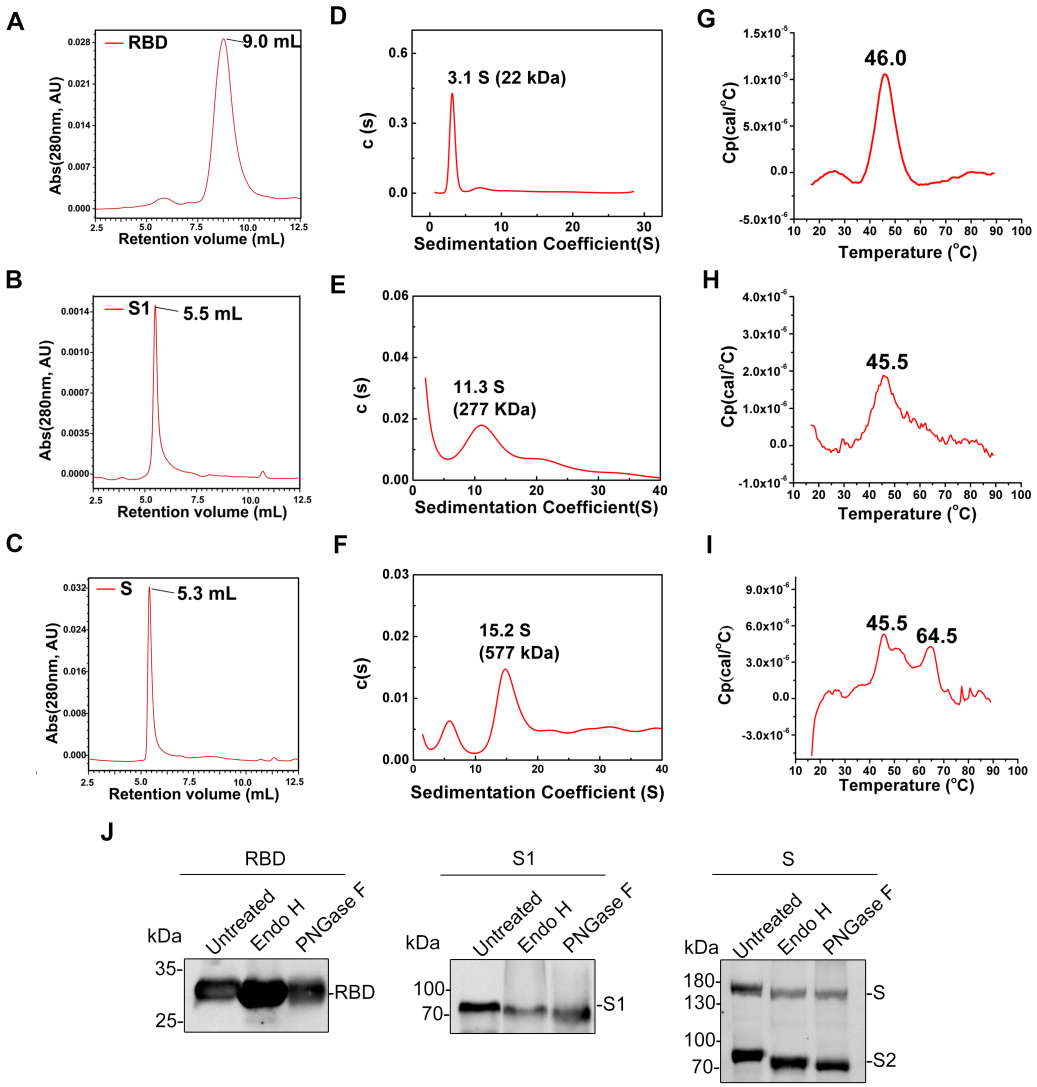

Figure 2. Characterization of the purified RBD, S1 and S proteins. (A-C) HPSEC profiles of the purified RBD, S1 and S proteins; (D-F) AUC profiles of RBD, S1 and S proteins; (G-I) DSC profiles of RBD, S1 and S proteins. (J) Western blotting of three purified proteins treated with Endo H and PNGase F or untreated as control. Anti-His antibody was used as detection antibody in western blotting.

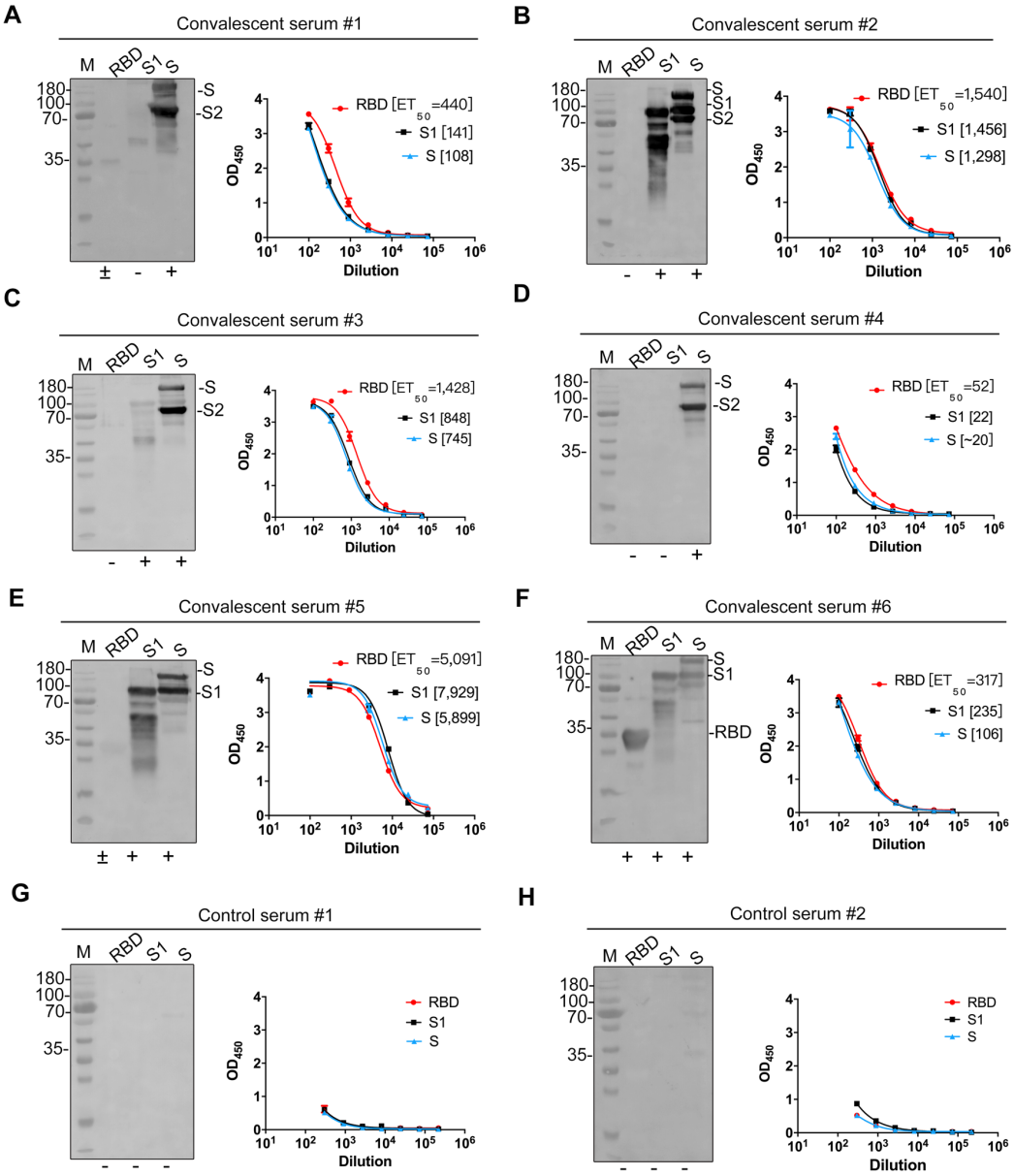

Figure 3. Antigenicity of RBD, S1 and S proteins against convalescent sera. (A-F) The reactivity of the RBD, S1 and S proteins against six COVID-19 convalescent human sera (#1-#6) by western blotting (left panel) and ELISA (Right panel). (G, H) Results of two control sera. The gels used for western blotting were duplicates of the reducing SDS gels same as Fig. 1C.

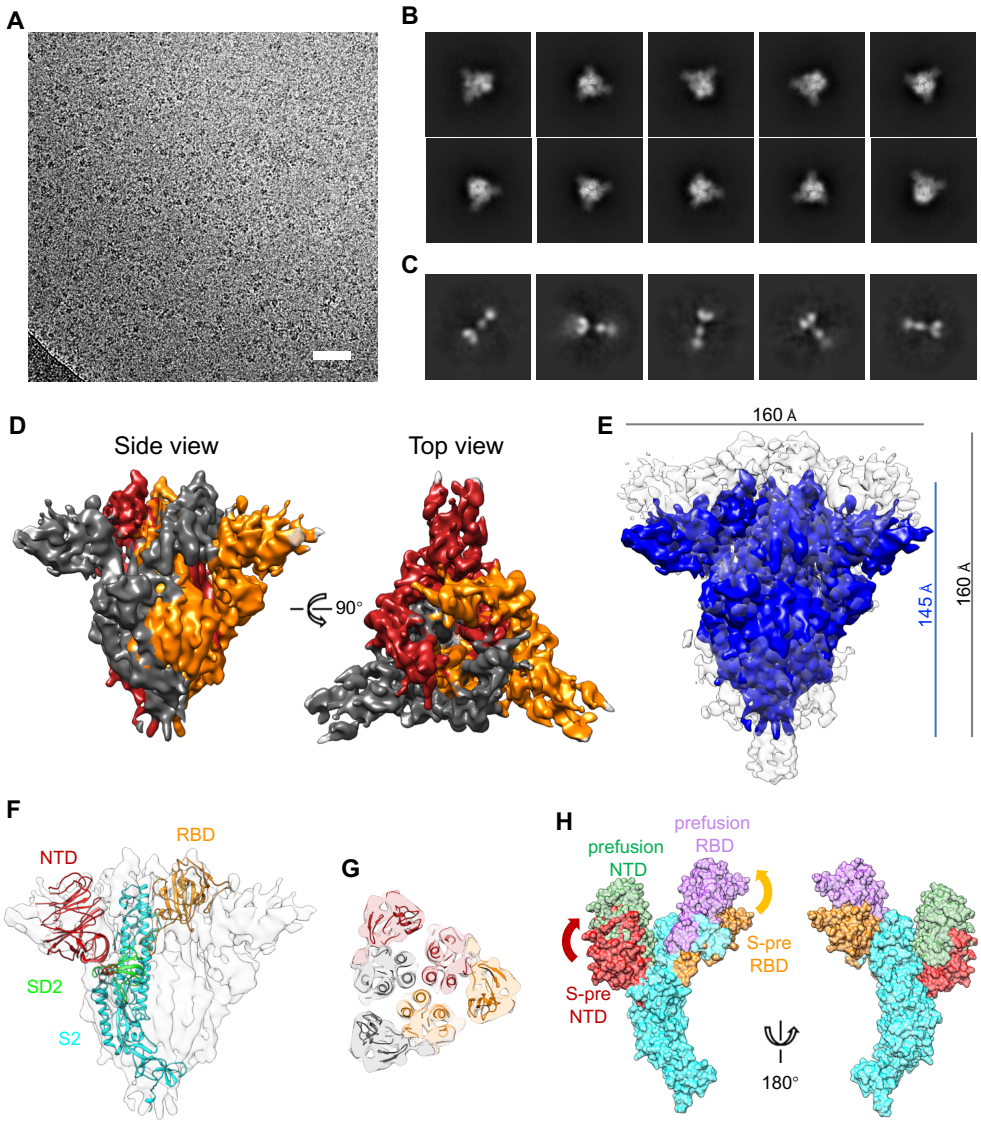

583

584 **Figure 4. Cryo-EM structure of the SARS-CoV-2 S trimer.** (A) Representative

585 micrograph of frozen-hydrated SARS-CoV-2 S particles, Scale bar 50nm. (B, C) Ten and five

586 selected class averages showing the particles along different orientations belonging to prefusion (B)

587 and postfusion (C) S protein, respectively. (D) 5.43 Å density map of prefusion S trimer (S-pre) that

588 is colored by protomer. (E) Structural comparison to the reported prefusion SARS-CoV-2 S trimer

589 (EMD-21374, C3 symmetry, low-pass to 5.43Å) show a different conformation of S-pre (~15Å

590 shorter in height). (F, G) Each domain of the model of prefusion SARS-CoV-2 S monomer (F) or

591 trimer (G) (PDB no. 6VSB) were separately fitted in the density map of S-pre. (H) Schematic

592 diagram shows conformational diversities between NTD and RBD of S-pre (NTD: red, RBD:

593 orange) and reported prefusion S (NTD: light green, RBD: light purple).

594

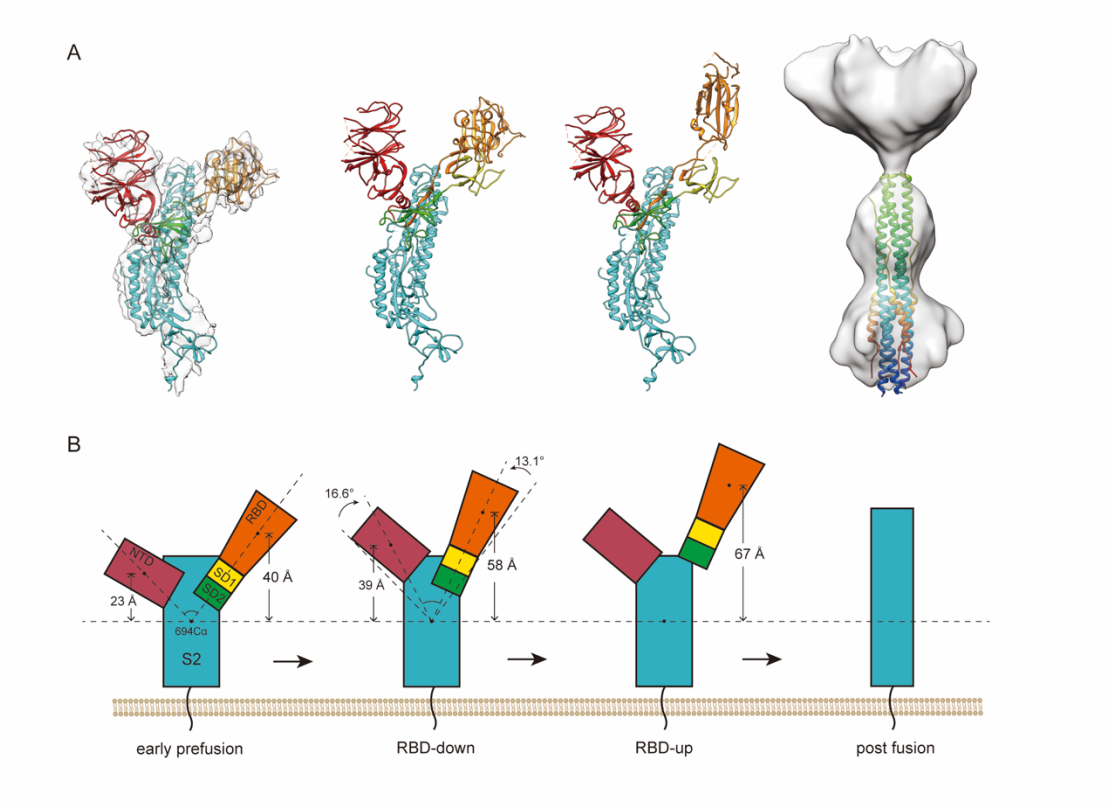

Figure 5. SARS-CoV-2 S spike at early pre-, pre- and post-fusion states and the proposed timeline for conformation change. (A) Four conformations of SARS-CoV-2 S spike. For clarity, only one monomer at early prefusion, RBD down prefusion and RBD up prefusion conformation is shown in ribbon mode. The model fitted in our S-pre map is a combined model comprised of individually fitted NTD, RBD, SD2 and S2 domain, which were evicted from the model of prefusion S trimer (PDB no. 6VSB). A deposited postfusion core of SARS-CoV-2 S2 subunit (PDB no. 6LXT) is fitted to our S-post map. Domains are designated by different colors, red: NTD, orange: RBD, yellow: SD1, green: SD2 and cyan: S2. (B) Simplified schematic diagram of the S monomer interpreting the conformation change across different states.

608 **Supplementary Information**

609 **Supplementary Figure 1**

610 **Supplementary Figure 2**

611 **Supplementary Figure 3**

612 **Supplementary Figure 4**

613 **Supplementary Movie 1**